Revista Brasileira de Geofísica
RBGf
Brazilian Journal of Geophysics

Revista Brasileira de Geofísica (2012) 30(1): 63-79
© 2012 Sociedade Brasileira de Geofísica
ISSN 0102-261X
www.scielo.br/rbg

PETROPHYSICAL MODEL FOR BULK DENSITY OF COMPLEX LITHOLOGIES

Mariana Ferreira de Magalhães[1] and Jorge Leonardo Martins[2]

Recebido em 29 março, 2011 / Aceito em 31 maio, 2012
Received on March 29, 2011 / Accepted on May 31, 2012

ABSTRACT. The workflow for an integrated well log analysis must incorporate physically-consistent models for rock properties prediction. Therefore, the selection of the conceptual model is a crucial step in deriving the petrophysical model under investigation. In this paper, we apply the parallel layers conceptual model to derive a petrophysical model for bulk density of complex lithologies. This conceptual model assumes the natural rock as a set of parallel layers with individual densities, incorporating the main factors affecting bulk density of sedimentary formations (i.e., the solid matrix, porosity and fluid content). The resulting petrophysical model shows the volumetric fractions of individual rock constituents as the key parameters for bulk density description. Further parameters of the dependence can be easily selected from petrophysical tables. In this way, evaluation of predefined volumetric fractions of rock constituents is a mandatory procedure for applying the investigated petrophysical model. We present results of calibration and estimation of bulk density well log measurements through turbiditic sediments forming the Namorado reservoir, Campos basin. In evaluating the facies-described volumetric fractions of main constituents of rocks at well surroundings, fundamental well log measurements represented the inputs for mineral volume analysis using the non-negative least-squares inversion method. The outcomes of both experiments exhibited the good performance of the petrophysical model in estimating bulk density with negligible absolute errors and high correlation coefficient. As a conclusion, the parallel layers conceptual model revealed enough robustness for construction of petrophysical models of other well log measurements.

Keywords: geophysical well logs, bulk density calibration and estimation, mineral volume analysis, Namorado reservoir.

RESUMO. O fluxo de trabalho para uma análise integrada de perfis de poços deve incorporar modelos fisicamente consistentes para a predição de propriedades de rochas. Portanto, a escolha do modelo conceitual é uma etapa crucial na derivação do modelo petrofísico sob investigação. Neste artigo, aplicamos o modelo conceitual baseado em camadas paralelas para derivar um modelo petrofísico para a densidade efetiva de litologias complexas. Este modelo conceitual assume a rocha natural como um conjunto de camadas paralelas com densidades individuais, incorporando os principais fatores que afetam a densidade efetiva de formações sedimentares (i.e., a matriz sólida, porosidade e conteúdo de fluidos). O modelo petrofísico resultante mostra as frações volumétricas dos constituintes individuais da rocha como os parâmetros principais para descrição da densidade efetiva. Parâmetros adicionais da dependência podem ser facilmente selecionados de tabelas petrofísicas. Dessa forma, a avaliação das frações volumétricas predefinidas para os constituintes da rocha é um procedimento mandatório para a aplicação do modelo petrofísico investigado. Apresentamos resultados da calibração e estimativa de medidas de densidade efetiva em perfil de poço através de sedimentos turbidíticos que formam o reservatório Namorado, bacia de Campos. Na avaliação das frações volumétricas dos principais constituintes das rochas na periferia do poço, medidas fundamentais de perfis de poço representaram os dados de entrada para análise volumétrica de minerais usando o método de inversão de mínimos quadrados não-negativos. Os resultados de ambos os experimentos exibiram a boa performance do modelo petrofísico na estimativa da densidade efetiva com erros absolutos negligenciáveis e alto coeficiente de correlação. Concluindo, o modelo conceitual baseado em camadas paralelas revelou robustez suficiente para construção de modelos petrofísicos de outras medidas de perfil de poço.

Palavras-chave: perfis geofísicos de poços, calibração e estimativa da densidade efetiva, análise volumétrica de minerais, reservatório Namorado.

[1]Departamento de Geologia, Instituto de Geociências, Universidade Federal Fluminense, Av. Gal. Milton Tavares de Souza, s/n, Campus da Praia Vermelha, Boa Viagem, 24210-340 Niterói, RJ, Brazil. Phone: +55(21) 2629-5944 – E-mail: marianamagalhaes@globomail.com

[2]Coordenação da Área de Geofísica, Observatório Nacional, Ministério da Ciência e Tecnologia, Rua Gal. José Cristino, 77, São Cristóvão, 20921-400 Rio de Janeiro, RJ, Brazil. Phone: +55(21) 3504-9233; Fax: +55(21) 2580-7081 – E-mail: jlmartins@on.br

INTRODUCTION

Geophysical well logs are routinely used in the identification of sedimentary formations possibly containing oil and gas accumulations. In exploration areas, interpretation of anomalies in well log measurements can indicate the potential of formations in accumulating hydrocarbons. Such results take part in the decision processes which either terminate exploration activities in the area or lead to the location of additional wells. On the other hand, in the management of an already delineated oil field, the assessment of the petrophysical properties of lithotypes forming the reservoirs is a requirement achieved by an integrated analysis of well logs. The full understanding of the oil field, the estimation of the fluid storing capacity and the optimization of the recovery methods for production increase are among the main goals in the development phase for field management. In this way, a detailed well log petrophysical analysis clearly represents a powerful procedure for risk mitigation during oil field development (Pennington, 2001).

In general, an integrated petrophysical analysis using well logs follows a quite orderly workflow. Basically, fundamental well logs take part in the interpretation procedures, aiming at estimating physical properties critical in reservoir characterization. For instance, a quick-look analysis of the anomalies in the lithology logs can reveal permeable zones. By correlating the lithology logs with electrical resistivity and porosity logs, fluid type in the correspondent permeable zone can be inferred (Dewan, 1983; Ellis & Singer, 2007). In order to proceed to the estimation of critical physical properties (i.e., shaliness, porosity and fluid saturation) in the zoned sedimentary intervals, crossplotting of physically-related log measurements and constructing histograms corroborate to the inferences obtained in the quick-look analysis (Dewan, 1983). At this point, the interpreter is able to decide for the best petrophysical model to apply for estimating the variation of a needed rock physical property at well surroundings.

Various of the petrophysical models currently available in well log interpretation for property estimation are mostly empirically designed (Ellis & Singer, 2007). Basically, a set of core plug measurements is used for establishing the coefficients of a selected mathematical equation through least-squares regression analysis (Augusto & Martins, 2009). The final form of the petrophysical model is that of the mathematical equation selected for implementing the least-squares regression. For instance, the empirical formula for shaliness estimation from gamma-ray logs in Larionov (1969) and in Clavier et al. (1977) use power and quadratic law, respectively, to determine the regression coefficients through least-squares method. As a further example, Archie's (1942) empirical formula for estimating water saturation in clay-free lithologies from electrical resistivity logs also incorporates power law into the regression procedure. Regarding clay-rich lithologies, the classical modified Archie's empirical formulas for estimating water saturation, i.e., the Indonesia equation (Poupon & Leveaux, 1971) and the Simandoux equation (Simandoux, 1963), combine power and quadratic laws to determine the regression coefficients. In fact, empirical models are crucially relevant in practice for prediction of key physical properties in well log interpretation. However, selection of an unsuitable mathematical equation for implementing the regression analysis can yield poor description of physical property dependence. In other words, in order to achieve a physically-consistent parameter dependence, the final form of the petrophysical model must incorporate solid physical concepts into its formulation by means of the so-called conceptual model.

In this paper, in order to represent a natural rock, we applied the conceptual model which proposes the description of effective physical properties by assuming the rock as parallel layers with individual physical properties (Schön, 1996). Such a conceptual model was used, for instance, in Wyllie et al. (1956), for deriving the time-average relationship for porosity estimation from P-wave sonic logs, and in Postma (1955) and Backus (1962), for estimating effective elastic stiffnesses of laminated solids. Based on the parallel layer conceptual model, we constructed a scheme for a natural rock holding the main components affecting measurements of physical properties (i.e., the solid matrix, the porous space and the fluid constituents). We then derived a volume-oriented petrophysical model for bulk density in which the final form is presented as an equation of weighted averages, incorporating volumetric fractions of rock constituents and additional parameters. In principle, determination of volumetric fractions of facies-described rock constituents is mandatory for practical application of the petrophysical model, while the additional physical parameters can be easily selected from petrophysical tables. Using a data set containing well log measurements and corresponding core log facies description, we applied the petrophysical model for calibration and estimation of bulk density in a turbiditic formation. In the calibration experiment, we assumed the bulk density measurements as integrant information in the non-negative least-squares inversion (Lawson & Hanson, 1974) of predefined volumetric fractions of rock-forming constituents. In the estimation experiment, we discarded the bulk density measurements from the non-negative least-squares inversion of volumetric fractions. The result of the calibration experiment was directly related to the well-posed nature of the linear system of equations inverted, providing negligible absolute errors with high

correlation coefficient (i.e., $r = 0.96$). On the other hand, although the estimation experiment generated an ill-posed linear system of equations, it also provided negligible absolute errors with plausible correlation coefficient (i.e., $r = 0.77$). The outcomes confirmed the robustness of the parallel layer conceptual model in the derivation of petrophysical models with physically-consistent parameter dependence.

METHODOLOGY

In the following, we introduce a petrophysical model for bulk density of complex lithologies. The model is derived on the basis of the parallel layer conceptual model, incorporating the main rock parameters affecting bulk density measurements. The consistence of the petrophysical model is demonstrated by specifications for mono-, bi- and polymineralic, clay-free and clay-rich, fluid-saturated sedimentary formations. However, the practical application of the model requires predefinition of rock constituents in terms of volumetric fractions. In order to obtain estimations of volumetric fractions of formation constituents from a geophysical well log data set, a least-squares based inversion method for mineral volume analysis is briefly summarized.

The petrophysical model for bulk density

The response of any geophysical logging tool is influenced by three main rock parameters (Dewan, 1983; Ellis & Singer, 2007): lithology (i.e., mineral composition), porosity and fluid saturation. In petrophysical terms, these are the parameters which influence on the effective physical property of rocks (Archie, 1950; Schön, 1996). Consequently, the formulation of a petrophysical model for any effective rock property must hold information on the relevant rock constituents. Keeping this principle as a rule, the following petrophysical model describes the bulk density of porous sedimentary rocks. It incorporates the individual contribution of the rock matrix and fluid components. As in Wyllie et al. (1958) and in Liner (2004), the solid matrix may contain several distinct grain minerals (e.g., quartz, feldspar, calcite and dolomite), clay minerals (e.g., kaolinite, illite, chlorite and smectite), a fraction of organic matter as in biogenetic sediments, and the lithologic cement. Fluid saturation may occur either individually or as a mixture of water, oil and gas. In order to clearly distinguish between grain minerals and clay minerals, hereafter we assume the definitions on grain size distribution proposed in Schön (1996). That is: clay minerals are small-scale grain minerals having mean diameter less than 6.3×10^{-2} mm, while minerals with mean grain diameter greater than 6.3×10^{-2} mm and less than 2.0 mm are effectively treated as grain minerals. Although crossplotting well log measurements can help in clay typing (Ellis & Singer, 2007), in the formulation below we refer to the rock constituent "CLAY" as "a mixture of silt and clay minerals". Furthermore, the lithologic cement is also considered as taking part of the rock constituents referred to as "grain minerals".

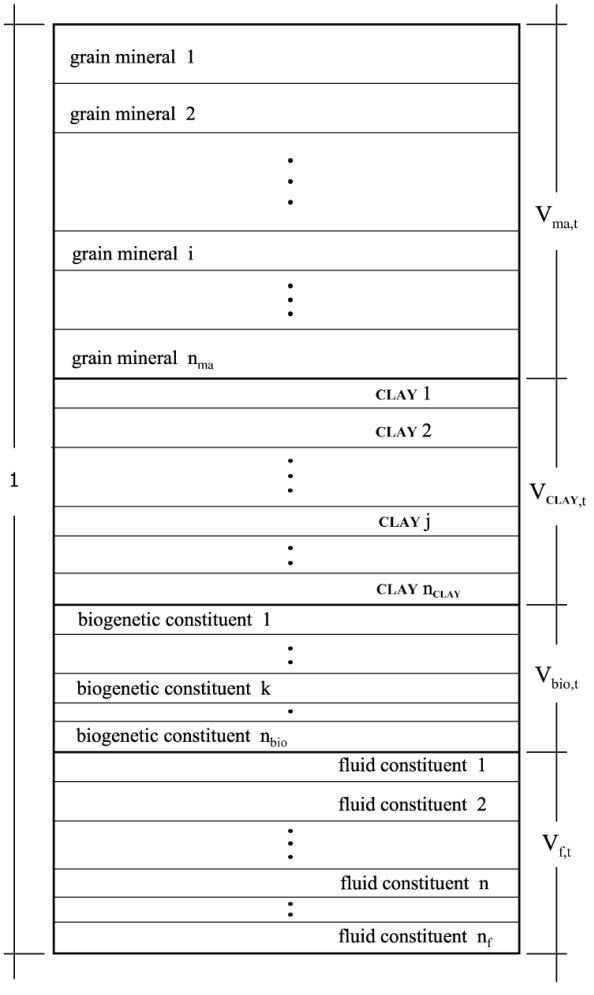

Figure 1 – Parallel layer conceptual model (Schön, 1996): scheme of a fluid-saturated porous rock used for derivation of the bulk density petrophysical model of sedimentary rocks in Eq. (1). As mentioned in the text, the rock constituent "CLAY" stands for "a mixture of silt and clay minerals". Note that, in assuming the rock 100 % saturated, the total volume fraction of fluid constituents $V_{f,t}$ coincides with the effective porosity ϕ_e.

In order to derive a petrophysical model for bulk density, we assume the parallel layer conceptual model depicted in Figure 1. According to Schön (1996), the parallel layer concept can provide description of effective physical properties by assuming the rock as parallel layers with individual physical properties. Using the parallel layer conceptual model, Magalhães & Martins (2008) proposed a petrophysical model for bulk density of sedimentary

formations. A modified version of Magalhães & Martins (2008) model is presented below as a sum of weighted averages of individual rock constituent,

$$\rho_{\rm b} = \bar{\rho}_{\rm ma} + \bar{\rho}_{\rm CLAY} + \bar{\rho}_{\rm bio} + \bar{\rho}_{\rm f}, \tag{1}$$

in which $(\bar{\rho}_{\rm ma} + \bar{\rho}_{\rm CLAY} + \bar{\rho}_{\rm bio})$ and $\bar{\rho}_{\rm f}$ denote the average density contribution of the rock matrix and fluids, respectively. As pointed out above, we consider the lithologic cement as an integrant part of the total density contribution of the grain minerals in the rock matrix, $\bar{\rho}_{\rm ma}$, expressed as

$$\bar{\rho}_{\rm ma} = (1 - {\rm V}_{\rm CLAY,t} - {\rm V}_{\rm bio,t} - \phi_{\rm e}) \times \left[\frac{1}{{\rm V}_{\rm ma,t}} \sum_{\rm i=1}^{\rm n_{ma}} {\rm V}_{\rm ma,i}\, \rho_{\rm ma,i} \right]. \tag{2}$$

In the preceding equation $\phi_{\rm e}$ is the fractional effective porosity, while ${\rm V}_{\rm ma,i}$ and $\rho_{\rm ma,i}$ are the volumetric fraction and the density, respectively, of the $\rm i^{th}$ predominant grain mineral ($\rm i = 1, 2, \ldots, n_{ma}$). The total volumetric fraction of the predominant grain minerals, ${\rm V}_{\rm ma,t}$, of the clay minerals, ${\rm V}_{\rm CLAY,t}$, and of the biogenetic rock constituent, ${\rm V}_{\rm bio,t}$, are respectively related as:

$${\rm V}_{\rm ma,t} = \sum_{\rm i=1}^{\rm n_{ma}} {\rm V}_{\rm ma,i}, \tag{3}$$

$${\rm V}_{\rm CLAY,t} = \sum_{\rm j=1}^{\rm n_{CLAY}} {\rm V}_{\rm CLAY,j}, \tag{4}$$

and

$${\rm V}_{\rm bio,t} = \sum_{\rm k=1}^{\rm n_{bio}} {\rm V}_{\rm bio,k}. \tag{5}$$

In Eqs. (4) and (5), ${\rm V}_{\rm CLAY,j}$ and ${\rm V}_{\rm bio,k}$ represent the volumetric fraction of the $\rm j^{th}$ rock-forming clay mineral ($\rm j = 1, 2, \ldots, n_{CLAY}$) and the volumetric fraction of the $\rm k^{th}$ biogenetic rock constituent ($\rm k = 1, 2, \ldots, n_{bio}$), respectively. Note that ${\rm V}_{\rm CLAY,\,t}$ is routinely addressed in practice as shaliness (i.e., the clay content), which is mainly estimated from lithologic well logs. For instance, Larionov (1969) presents empirical formulas for shaliness estimation using gamma-ray (GR) log measurements. For unconsolidated sediments, Larionov's empirical formula for shaliness reads

$${\rm V}_{\rm CLAY}^{\rm GR} = 0.083 \left(2^{\,3.70 \times {\rm IGR}} - 1 \right), \tag{6}$$

in which the gamma-ray index

$${\rm IGR} = ({\rm GR_i} - {\rm GR_{ss}})/({\rm GR_{sh}} - {\rm GR_{ss}}),$$

with $\rm GR_i$ denoting the $\rm i^{th}$ GR log measurement. For the same formation under study, the quantities $\rm GR_{ss}$ and $\rm GR_{sh}$ represent the minimum and maximum readings in the gamma-ray log taken in the sandstone and in the shale point, respectively (Dewan, 1983; Ellis & Singer, 2007). In the experiments below, we deal with well log measurements of an unconsolidated turbiditic formation, i.e., the upper Macaé formation. Hence, we apply Eq. (6) for shaliness estimation from GR measurements.

The additional total average contributions in Eq. (1), i.e., $\bar{\rho}_{\rm CLAY}$, $\bar{\rho}_{\rm bio}$ and $\bar{\rho}_{\rm f}$, are related in the following. The total average contribution of the clay minerals $\bar{\rho}_{\rm CLAY}$ forming the rock matrix is expressed as

$$\bar{\rho}_{\rm CLAY} = \sum_{\rm j=1}^{\rm n_{CLAY}} {\rm V}_{\rm CLAY,j}\, \rho_{\rm CLAY,j}, \tag{7}$$

the total average contribution of organic constituents $\bar{\rho}_{\rm bio}$ in the rock matrix, is written as

$$\bar{\rho}_{\rm bio} = \sum_{\rm k=1}^{\rm n_{bio}} {\rm V}_{\rm bio,k}\, \rho_{\rm bio,k}, \tag{8}$$

and the formula for the total average density contribution of the fluids $\bar{\rho}_{\rm f}$ saturating the porous of the rock is

$$\bar{\rho}_{\rm f} = \phi_{\rm e} \sum_{\rm n=1}^{\rm n_f} {\rm S}_{\rm f,n}\, \rho_{\rm f,n}, \tag{9}$$

where ${\rm S}_{\rm f,\,n}$ and $\rho_{\rm f,\,n}$ denote the saturation and density, respectively, of the $\rm n^{th}$ ($\rm n = 1, 2, \ldots, n_f$) fluid constituent.

Once the effective porosity as well as the volumetric fractions of solid and fluid constituents are available, the petrophysical model in Eq. (1) allows evaluating bulk density of monomineralic and polymineralic porous sedimentary rocks. In the following, we specify Eq. (1) to some practical models for evaluating bulk density of monomineralic and polymineralic clastic reservoir rocks. Conversely, we obtain general relations for total and effective porosity estimation from bulk density logs.

Monomineralic clay-free sandstones – Let us consider a 100% water-saturated clay-free sandstone with no biogenetic constituent. Using the terminology as above, we write ${\rm V}_{\rm CLAY,t} = {\rm V}_{\rm bio,t} = 0$ and ${\rm S_w} = 1$. Since we deal with a clean sandstone, the total porosity $\phi_{\rm t}$ better represents the rock porous space rather than the effective porosity $\phi_{\rm e}$. As a result, Eq. (1) then reduces to

$$\rho_{\rm b} = (1 - \phi_{\rm t})\, \rho_{\rm ma} + \phi_{\rm t}\, \rho_{\rm w}, \tag{10}$$

where ρ_{ma} and ρ_w are the density of the grain mineral in the rock matrix and of the water saturating the porous of the rock, respectively. Eq. (10) represents the model for the response of the bulk density logging tool. In this instance, ρ_w is indeed the density of the mud filtrate saturating the so-called flushed zone (Dewan, 1983). Further, a simple manipulation of Eq. (10) yields the formula routinely used for estimating fractional total porosity from bulk density log measurements,

$$\phi_t = \frac{\rho_{ma} - \rho_b}{\rho_{ma} - \rho_w}. \tag{11}$$

Note that application of Eq. (11) in the estimative of fractional total porosity necessarily implies that bulk density measurements ρ_b are performed in the flushed zone.

Monomineralic clay-rich sandstones – For the case of a clay-rich sandstone, we assume the shaliness as the total volumetric fraction of clay minerals in the rock, that is, $V_{CLAY} = V_{CLAY,t}$. Furthermore, the sandstone is free from biogenetic constituents ($V_{bio,t} = 0$) and 100% water-saturated ($S_w = 1$). Under these assumptions, Eq. (1) reduces to

$$\begin{aligned}\rho_b = (1 - V_{CLAY} - \phi_e)\,\rho_{ma} \\ + V_{CLAY}\,\rho_{CLAY} + \phi_e\,\rho_w.\end{aligned} \tag{12}$$

The concept of effective porosity ϕ_e is now taking into account, because of the assumption that clay minerals obstruct the connections between the porous of the rock. In other words, clay minerals are found dispersed in the rock matrix (Dewan, 1983). As long as shaliness V_{CLAY} can be estimated, for instance, from GR log measurements, manipulation of Eq. (12) gives the formula commonly applied in the estimation of effective porosity from bulk density logs. That is,

$$\phi_e = \phi_t - V_{CLAY}\,\frac{\rho_{ma} - \rho_{CLAY}}{\rho_{ma} - \rho_w}, \tag{13}$$

where ϕ_t is expressed in Eq. (11). In practice, the term ρ_{CLAY} represents the density at the shale point (i.e., at the adjacent shale in the formation under study). In order to assess the density at the shale point, we can simply take the difference between the neutron porosity log and the total porosity log at its maximum, i.e., $\max(\phi_{N,i} - \phi_{t,i})$, where $\phi_{N,i}$ and $\phi_{t,i}$ correspond to the i^{th} sample of the neutron porosity and the total porosity logs, respectively (Dewan, 1983). In Eq. (13), the quotient which follows V_{CLAY} is defined as the apparent porosity at the shale point, that is, $\phi_{CLAY} \equiv (\rho_{ma} - \rho_{CLAY})/(\rho_{ma} - \rho_w)$. Therefore, the relation for effective porosity in Eq. (13) can be interpreted as the shaliness correction of total porosity using the apparent porosity at the shale point. The densities ρ_{ma} and ρ_w hold the same corresponding concepts presented in the derivation of Eq. (11).

Bimineralic clay-free sandstones – The petrophysical model for the bulk density of a bimineralic clay-free sandstone requires the volumetric fractions of corresponding grain minerals forming the rock matrix. Thus, using the terminology as above, $V_{ma,i}$ as well as the density of grain minerals $\rho_{ma,i}$ are known quantities. For a 100% water-saturated sandstone ($S_w = 1$), with matrix having no biogenetic constituent ($V_{bio,t} = 0$) and formed only by quartz and feldspar, Eq. (1) yields

$$\rho_b = (1 - \phi_t)\left[\frac{V_{qtz}\,\rho_{qtz} + V_{felds}\,\rho_{felds}}{V_{ma,t}}\right] + \phi_t\,\rho_w. \tag{14}$$

In agreement with Eq. (3), $V_{ma,\,t} = V_{qtz} + V_{felds}$. The volumetric fractions of quartz and feldspar (i.e., V_{qtz} and V_{felds}, respectively) reflect the weights of the contributions of each type of grain mineral in the rock matrix. Once both V_{qtz} and V_{felds} as well as the density of the quartz, ρ_{qtz}, and the density of the feldspar, ρ_{felds}, are known quantities, a more complex equation for total porosity can be derived from Eq. (14), namely,

$$\phi_t = \frac{(V_{qtz}\,\rho_{qtz} + V_{felds}\,\rho_{felds})/V_{ma,t} - \rho_b}{(V_{qtz}\,\rho_{qtz} + V_{felds}\,\rho_{felds})/V_{ma,t} - \rho_w}. \tag{15}$$

Use of Eq. (15) implies that ρ_b and ρ_w represent the bulk density log and the mud filtrate density, respectively.

Inspection of Eq. (15) shows that the formula for total porosity can be easily generalized for the case of a polymineralic sandstone free from clay minerals. The generalization yields

$$\phi_t = \frac{(1/V_{ma,t})\sum_{i=1}^{n_{ma}} V_{ma,i}\,\rho_{ma,\,i} - \rho_b}{(1/V_{ma,t})\sum_{i=1}^{n_{ma}} V_{ma,i}\,\rho_{ma,i} - \rho_w}, \tag{16}$$

where now Eq. (3) applies for calculating $V_{ma,\,t}$. However, without precisely knowledge of volumetric fractions of grain minerals and corresponding densities, use of Eq. (16) in the estimation of total porosity from bulk density logs is clearly impractical.

Bimineralic clay-rich sandstones – In addition to the volumetric fractions of the grain minerals contained in the rock matrix, the volumetric fractions of clay minerals are also required for obtaining the corresponding bulk density model for a bimineralic clay-rich sandstone. Similarly as in Eq. (14), we assume a 100% water-saturated sandstone ($S_w = 1$) with matrix having no biogenetic constituent ($V_{bio,t} = 0$) and formed only by quartz and feldspar. However, we additionally consider clay minerals obstructing the connections between pores, which implies in using the concept of effective porosity ϕ_e. Taking these assumptions into account, Eq. (1) yields the bulk density model of

a bimineralic clay-rich sandstone

$$\rho_b = (1 - V_{CLAY} - \phi_e)\left[\frac{V_{qtz}\rho_{qtz} + V_{felds}\rho_{felds}}{V_{ma,t}}\right] + V_{CLAY}\,\rho_{CLAY} + \phi_e\,\rho_w, \quad (17)$$

where V_{CLAY} and ρ_{CLAY} denote clay minerals volumetric fraction and density, respectively. The sum $V_{ma,\,t} = V_{qtz} + V_{felds}$ also applies to Eq. (17).

In this instance, an expression similar to Eq. (13) for effective porosity estimation of bimineralic clay-rich sandstones from bulk density logs can be derived. Rearranging Eq. (17), we write

$$\phi_e = \phi_t - V_{CLAY} \times \frac{(V_{qtz}\,\rho_{qtz} + V_{felds}\,\rho_{felds})/V_{ma,t} - \rho_{CLAY}}{(V_{qtz}\,\rho_{qtz} + V_{felds}\,\rho_{felds})/V_{ma,t} - \rho_w}, \quad (18)$$

where now ϕ_t is given by Eq. (15). In the preceding equation, ρ_{CLAY} can be assumed as the average density of the clay minerals forming the solid portion of the rock. Clearly, Eq. (18) can be generalized as

$$\phi_e = \phi_t - V_{CLAY} \times \frac{(1/V_{ma,t})\sum_{i=1}^{n_{ma}} V_{ma,i}\,\rho_{ma,i} - \rho_{CLAY}}{(1/V_{ma,t})\sum_{i=1}^{n_{ma}} V_{ma,i}\,\rho_{ma,i} - \rho_w}, \quad (19)$$

which theoretically allows estimation of fractional effective porosity of polymineralic clay-rich sandstones. In this instance, the total porosity ϕ_t is given by Eq. (16).

In order to apply the petrophysical model for bulk density in Eq. (1) and the derived relations above, the volumetric fractions of the rock constituents must be known beforehand. These parameters can be evaluated in practice using a technique called mineral volume analysis, which is detailed in the following section.

Mineral volume analysis

In order to predict bulk density of sedimentary rocks using the petrophysical model in Eq. (1), three basic steps are required: (1) description of predominant (i.e., solid and fluid) rock constituents, (2) selection of intrinsic densities of the predominant rock constituents, and (3) determination of correspondent volumetric fractions of rock constituents. If the objectives of the study require a higher accuracy in the description of rock constituents, the first step is generally performed in a well-structured petrophysics laboratory. On the other hand, if a coarse description of rock constituents is enough for the investigation, the first step can be performed visually by an experimented sedimentary geologist. For instance, this is the case in well drilling operations where cuttings are submitted to a quick-look description of texture and main mineral constituents. Tables of physical properties can then help defining the densities of rock constituents described in the first step. However, of fundamental importance in the application of the petrophysical model as presented above are the estimation of volumetric fractions of rock constituents identified in the first step.

The most common technique used for estimating volumetric fractions of rock-forming minerals takes cores and/or well log measurements as inputs (Doveton, 1994). The technique implements a mineral volume analysis based on the principle that a logging tool reading is the response of three individual parts of formation constituents: minerals, porosity and fluids. Taking this principle into account, the formulation for inverting mineral volumetric fractions starts by assuming $\mathbf{m}_{k,\,i}$ as the i^{th} measurement from the k^{th} selected well log ($k = 1, 2, \ldots, N$). The mass balance equation is then written as

$$\mathbf{m}_{k,i} = \sum_{j=1}^{n_c} \mathbf{m}_{k,j}\,\mathbf{V}_j, \quad (20)$$

which can also be viewed as a measurement of $\mathbf{m}_{k,i}$ performed in the rock model depicted in Figure 1. In other words, the log measurement represents the sum of proportions of the considered rock constituents. The term $\mathbf{m}_{k,j}$ denotes the measurement of the corresponding logging tool for the lithology solely formed by the j^{th} rock constituent, while $\mathbf{V}_j$ corresponds to the volumetric fraction of the j^{th} rock constituent ($j = 1, 2, \ldots, n_c$).

A system of linear equations arises from expanding the summation in Eq. (20). If a suitable set of well logs is used as input, the resulting system allows estimation of the volumetric fractions $\mathbf{V}_j$. In matrix form, the system of linear equations can be expressed as

$$\mathbf{r} = \mathbf{M}\,\mathbf{v}. \quad (21)$$

The vector $\mathbf{r}$ contains measurements of the selected well logs, i.e.,

$$\mathbf{r} = \begin{bmatrix} \mathbf{m}_{1,i} & \mathbf{m}_{2,i} & \mathbf{m}_{3,i} & \cdots & \mathbf{m}_{N,i} & 1 \end{bmatrix}^T, \quad (22)$$

in which the symbol $[\,\bullet\,]^T$ stands for transpose operation. The vector of unknowns, which elements are the j^{th} volumetric fraction associated to the predefined rock constituents, can be written as

$$\mathbf{v} = \begin{bmatrix} V_1 & V_2 & V_3 & \cdots & V_{n_c} \end{bmatrix}^T, \quad (23)$$

and matrix $\mathbf{M}$, with $(\mathrm{N}+1)$ rows and $\mathrm{n_c}$ columns, has the following structure

$$\mathbf{M} = \begin{bmatrix} \mathbf{m}_{1,1} & \mathbf{m}_{1,2} & \cdots & \mathbf{m}_{1,\mathrm{n_c}} \\ \mathbf{m}_{2,1} & \mathbf{m}_{2,2} & \cdots & \mathbf{m}_{2,\mathrm{n_c}} \\ \vdots & \vdots & \vdots & \vdots \\ \mathbf{m}_{\mathrm{k},1} & \mathbf{m}_{\mathrm{k},2} & \cdots & \mathbf{m}_{\mathrm{k},\mathrm{n_c}} \\ \vdots & \vdots & \vdots & \vdots \\ \mathbf{m}_{\mathrm{N},1} & \mathbf{m}_{\mathrm{N},2} & \cdots & \mathbf{m}_{\mathrm{N},\mathrm{n_c}} \\ 1 & 1 & \cdots & 1 \end{bmatrix}. \qquad (24)$$

The elements of $\mathbf{M}$ are constants selected from tables of petrophysical properties (i.e., Schlumberger Log Interpretation Charts, 2009 Edition).

In order to solve Eq. (21), the least-squares (LS) method is classically used in the literature (see, for instance, Lawson & Hanson, 1974; Paige & Saunders, 1982; Lines & Treitel, 1984). Nevertheless, the estimated solution $\mathbf{v}^{\mathrm{est}}$ may be unstable if the number of equations $(\mathrm{N}+1)$ is less than the number of unknowns $\mathrm{n_c}$. That is, the system is underdetermined because there are no enough well logs for resolving the unknowns. Still, an underdetermined system may be additionally inconsistent, yielding a solution with non-physical values. In the current instance, the volumetric fractions of rock constituents can show negative values. To deal with possibly underdetermined inconsistent systems of equations, we apply the so-called LS with linear inequality constraints described in Lawson & Hanson (1974). The LS method with linear inequality constraints, which is referred to as LSI, is a reformulation of the classical LS method (Levenberg, 1944; Marquardt, 1963) introducing information on the problem in the form of inequality constraints. A particular case of LSI applies to Eq. (21), in which negative values for the estimated solution $\mathbf{v}^{\mathrm{est}}$ are unacceptable. The algorithm is named non-negative least squares (NNLS) and is simply formulated as

$$\text{Minimize } \| \mathbf{M}\,\mathbf{v} - \mathbf{r} \|, \qquad \text{subject to} \qquad \mathbf{v} \geq 0, \qquad (25)$$

where $\mathbf{v} \equiv \mathbf{v}^{\mathrm{est}}$ and $\| \bullet \|$ stands for the Euclidian norm. According to Lawson & Hanson (1974), the NNLS algorithm converges to a stable solution in $\mathrm{n_c}/2$ iterations. The results in the following section confirms the robustness of NNLS in giving a stable solution $\mathbf{v}^{\mathrm{est}}$ for the system in Eq. (21).

RESULTS

This section shows the outcomes of two experiments involving the application of the petrophysical model in Eq. (1), that is: calibration and estimation of bulk density. Both experiments rely on continuous measurements of petrophysical data at the surroundings of a vertical well through a turbiditic oil-bearing sandstone reservoir in Campos basin, Brazil. Core log lithologic description is also available, allowing definition of the volumetric fractions $\mathbf{V}_{\mathrm{j}}$'s and selection of $\mathbf{m}_{\mathrm{k,j}}$'s for inverting the system in Eq. (21). The data set as well as the experiments with bulk density calibration and estimation are presented in the following subsections.

The data set

In this paper, the set of information used in the calibration and estimation of bulk density log refers to a vertical well through the Namorado sandstone reservoir. As shown in Figure 2, the well NA04 is located in the southeastern part of the reservoir structural map. Of turbiditic origin, the oil-producing Namorado reservoir is embedded in the upper Macaé formation, from 2940 to 3300 m depth. Complex lithologies form the reservoir facies, containing poorly consolidated sandstones alternated by thin layers of calcareous shales, siltstones and calcilutites (Tigre & Lucchesi, 1986). In Figure 3, fundamental well log measurements from 3025 to 3125 m depth exhibit variations of physical properties of lithotypes at the surroundings of well NA04. Inspection of GR log anomalies in Figure 3a shows high radioactivity even in the two major oil-producing sandstone intervals. In the subsequent displays, the neutron porosity (ϕ_N), bulk density (ρ_{b}) and P-wave sonic ($\Delta \mathrm{t}_P$) logs at well NA04 provide a means of correlating depth anomalies in log measurements. In addition to the well logs in Figure 3, sequential analysis of five cores – see Figure 4 – extracted from specific depths of well NA04 describes lithology and mineral constituents. The summary of the sequential analysis in Table 1 reveals that the Namorado sandstone is of arcosean nature (i.e., the reservoir is rich in K-feldspar).

As a result of the core log lithology description in Table 1, grain minerals (i.e., quartz, K-feldspar and calcite) and clay minerals are the predominant solid constituents of upper Macaé formation. The occurrence of biogenetic constituents is insignificant to take into account in the mineral volume analysis, because the source rocks are far below the formation under study. In this way, the components of vector $\mathbf{v}$ in Eq. (21) are volumetric fractions of the formation constituents, i.e.,

$$\mathrm{V}_1 \equiv \mathrm{V}_{\mathrm{fluid}},\ \mathrm{V}_2 \equiv \mathrm{V}_{\mathrm{qtz}},\ \mathrm{V}_3 \equiv \mathrm{V}_{\mathrm{felds}},$$
$$\mathrm{V}_4 \equiv \mathrm{V}_{\mathrm{calc}} \quad \text{and} \quad \mathrm{V}_5 \equiv \mathrm{V}_{\mathrm{CLAY}}.$$

In vector notation,

$$\mathbf{v} = \begin{bmatrix} \mathrm{V}_{\mathrm{fluid}} & \mathrm{V}_{\mathrm{qtz}} & \mathrm{V}_{\mathrm{felds}} & \mathrm{V}_{\mathrm{calc}} & \mathrm{V}_{\mathrm{CLAY}} \end{bmatrix}^{\mathrm{T}}. \qquad (26)$$

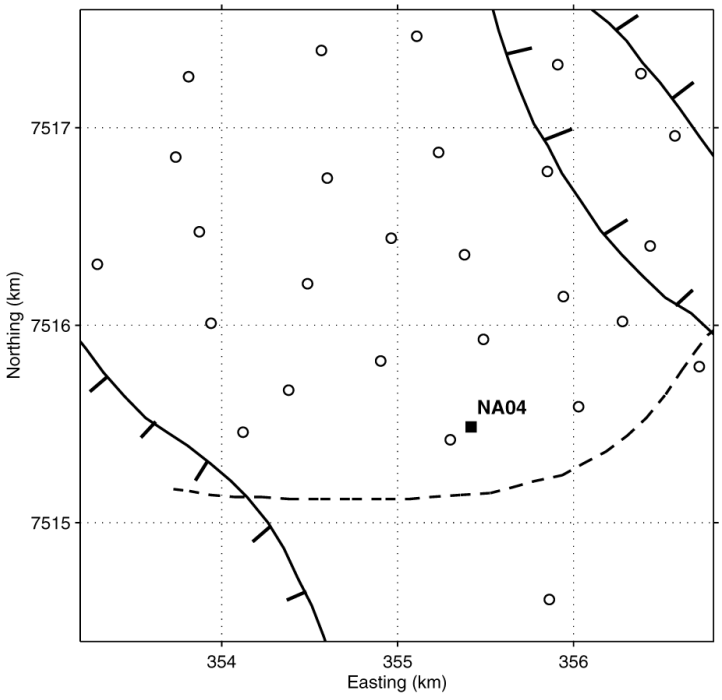

Figure 2 – Portion of the structural map of Namorado oil field in Campos basin, Brazil. The filled square locates the selected well, named NA04. Further drilled wells in the area are marked with circles. The reservoir bounds are shown by lateral normal faults and a dashed line in the easting direction.

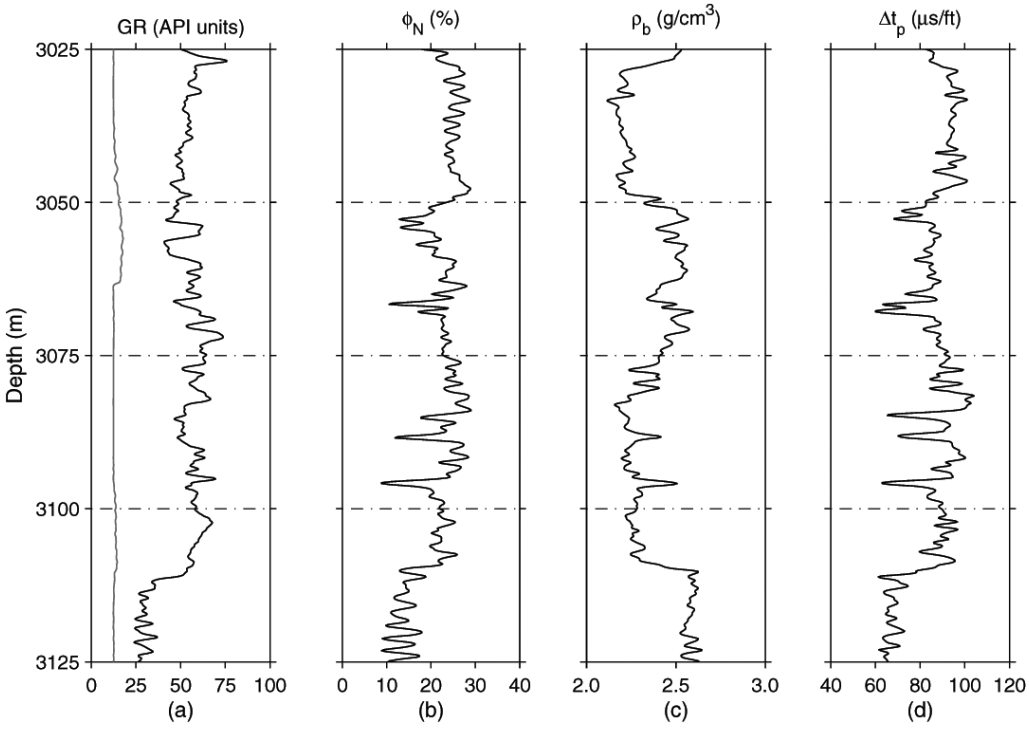

Figure 3 – Geophysical well logs at well NA04. (a) Caliper (left curve, in inches) and natural gamma-ray (GR, in API units) logs. (b) Neutron porosity (ϕ_N, in %) log. (c) Bulk density (ρ_b, in g/cm^3) log. (d) Compressional-wave sonic (Δt_p, in μs/ft) log. Corresponding log units are in the top of each plot. The caliper log is shown in inches. In order to correlate oil intervals with mineral volumes, Figures 7a and 9a show the induction electrical resistivity (R_{ild}, in Ohm.m) log at well NA04.

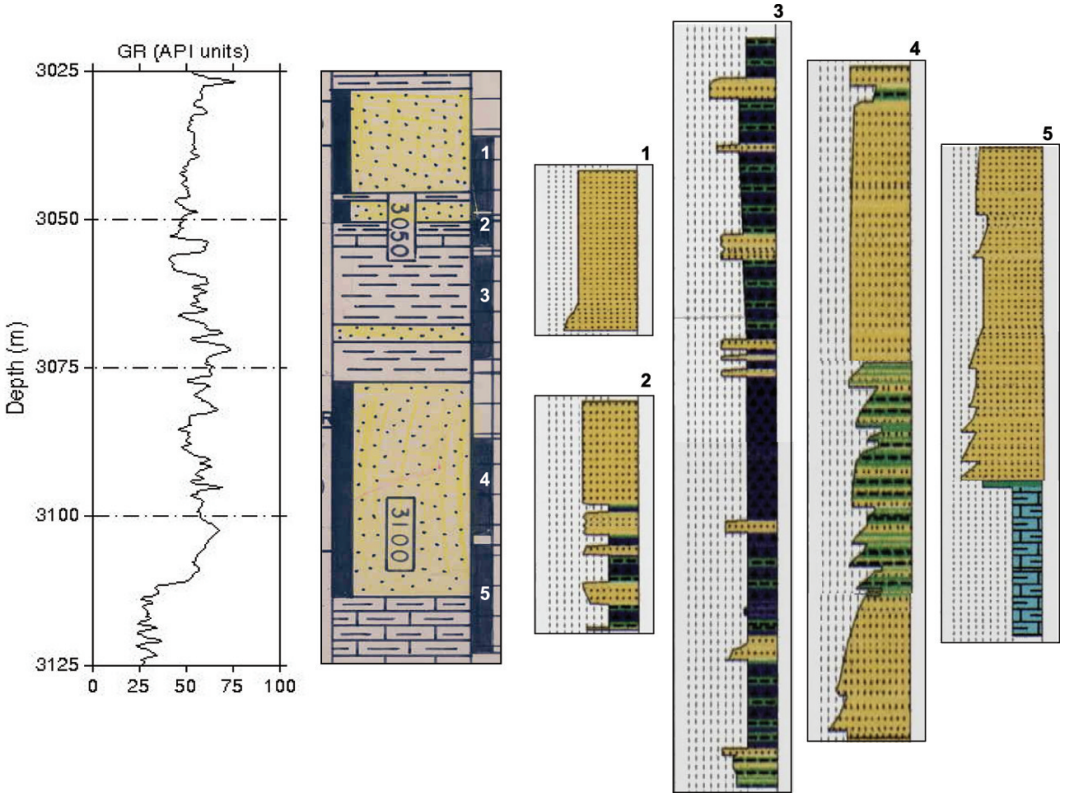

Figure 4 – The lithology column and location of cores at well NA04. The display of the lithology column corresponds to the same depth interval of the GR log. Table 1 shows a summary of facies description as well as the main mineral constituents resulting from core log sequential analysis.

Table 1 – Summary of core log sequential analysis: facies description using cores extracted from the depth intervals shown in Figure 4. The sequential analysis reveals insignificant occurrence of biogenetic constituents, because the source rocks are far below the upper Macaé formation. In order to represent "a mixture of silt and clay minerals", the term "CLAY" is used.

Core	Depth interval (m)	Facies description	Main constituents
1	3036.50–3042.80	Well sorted arcosean sandstone.	quartz, K-feldspar
2	3048.00–3053.90	Well sorted arcosean sandstone (top); interlaminations of clayey silt (bottom).	quartz, K-feldspar, CLAY
3	3055.50–3072.70	Intercalations of cemented, clay-rich, arcosean sandstone; interlaminations of clayey silt and bioturbated calcareous shale (35-50% $CaCO_3$ content).	quartz, K-feldspar, calcite, CLAY
4	3086.50–3100.80	Cemented arcosean sandstone with intermediate laminations of clayey silt.	quartz, K-feldspar, CLAY
5	3103.50–3119.50	Cemented arcosean sandstone (top); carbonate-rich interval (bottom), with interlaminations and rhythmic intercalations of calcilutite, calcareous shales (35-50% $CaCO_3$ content) and shale.	quartz, K-feldspar, calcite, CLAY

Note that the assumption of well log measurements in the flushed zone leads to $\phi_e \equiv V_{fluid}$. In other words, the volumetric fraction of fluid (i.e., the mud filtrate) saturating the lithologies in the flushed zone is equivalent to the fractional effective porosity. Moreover, $V_{qtz} + V_{felds} + V_{calc} + V_{CLAY} + V_{fluid} = 1$.

Hence, the mineral volume inversion worked with systems of five columns (i.e., $n_c = 5$). Next sections show that the number of equations depends on the number of well logs available for calibration and estimation of bulk density using the petrophysical model in Eq. (1).

Bulk density calibration

We use the data set described above for calibrating bulk density log measured at well NA04, using the petrophysical model in Eq. (1). However, for the application of the petrophysical model, inversion of volumetric fractions as defined in vector (26) is a requirement. In this instance, the components of vector $\mathbf{r}$ correspond to the i^{th} measurement of the compressional-wave sonic, bulk density, gamma-ray and neutron-porosity logs, i.e.,

$$\mathbf{r} = \begin{bmatrix} \Delta t_{log,i} & \rho_{b,log,i} & GR_{log,i} & \phi_{N,log,i} & 1 \end{bmatrix}^T. \quad (27)$$

That is, the elements of vector $\mathbf{r}$ represent the inputs for solving the linear system in Eq. (21). Note that we discarded the induction electrical resistivity log, because such measurements are far away from the zone of interest (i.e., the flushed zone). Only micro-resistivity logging tools have depth of penetration in the flushed zone (Ellis & Singer, 2007). Unfortunately, micro-resistivity log measurements are unavailable in the data set of well NA04.

As pointed out above, the elements of matrix $\mathbf{M}$ in the linear system Eq. (21) are the response of the correspondent logging tool to formation constituents. Regarding the constituents of the formation at well NA04 described in Table 1, matrix $\mathbf{M}$ takes the following form

$$\mathbf{M} = \begin{bmatrix} \Delta t_{fluid} & \Delta t_{qtz} & \Delta t_{felds} & \Delta t_{calc} & \Delta t_{CLAY} \\ \rho_{b,fluid} & \rho_{b,qtz} & \rho_{b,felds} & \rho_{b,calc} & \rho_{b,CLAY} \\ GR_{fluid} & GR_{qtz} & GR_{felds} & GR_{calc} & GR_{CLAY} \\ \phi_{N,fluid} & \phi_{N,qtz} & \phi_{N,felds} & \phi_{N,calc} & \phi_{N,CLAY} \\ 1 & 1 & 1 & 1 & 1 \end{bmatrix} \quad (28)$$

Most of the elements of matriz $\mathbf{M}$ can be easily taken from petrophysical tables. However, a critical procedure concerns the selection of "CLAY" physical properties, because several clay minerals can be present in the formation under study. The procedures used in this paper to select "CLAY" physical properties are described in Table 2. The additional physical properties were taken from the Schlumberger Log Interpretation Charts, 2009 Edition. In this instance, the linear system in Eq. (1) can be written as (see Table 2)

$$\begin{bmatrix} \Delta t_{log,i} \\ \rho_{b,log,i} \\ GR_{log,i} \\ \phi_{N,log,i} \\ 1 \end{bmatrix} = \begin{bmatrix} 185.00 & 55.500 & 69.000 & 48.100 & 85.00 \\ 1.10 & 2.650 & 2.540 & 2.710 & 2.56 \\ 0.00 & 1.000 & 171.000 & 12.000 & 59.00 \\ 1.00 & -0.018 & -0.006 & 0.002 & 0.24 \\ 1.00 & 1.000 & 1.000 & 1.000 & 1.00 \end{bmatrix} \times \begin{bmatrix} V_{fluid} \\ V_{qtz} \\ V_{felds} \\ V_{calc} \\ V_{CLAY} \end{bmatrix}, \quad (29)$$

of which the inversion gives estimations of the volumetric fractions of formation constituents at well NA04 as defined in vector (26).

Table 2 – Physical values for log response of lithologies at well NA04. (a) Bulk density calibration experiment: selection of "CLAY" properties at the shale point using the procedure after Eq. (13). (b) Bulk density estimation experiment: selection of the average of the sonic log ($\Delta t_{P,CLAY} = 86\,\mu$s/ft), the maximum of the gamma-ray log ($GR_{CLAY} = 76$ API units), and the maximum of the neutron porosity log ($\phi_{N,CLAY} = 29\,\%$). Substituting the density-derived total porosity log $\phi_{t,D}$ by the sonic-derived total porosity log $\phi_{t,S} = (\Delta t_{qtz} - \Delta t\rho)/(\Delta t_{qtz} - \Delta t_{fluid})$, the procedure after Eq. (13) yields $\rho_{CLAY} = 2.54$ g/cm^3 – a result nearly the same as in CLAY(a). Additional physical properties for rock constituents selected from the Schlumberger Log Interpretation Charts, 2009 Edition.

Rock constituents	Log response			
	Δt_P (μ s/ft)	ρ (g/cm^3)	GR (API units)	ϕ_N (%)
fluid	185.00	1.10	0.00	100.00
quartz	55.50	2.65	1.00	–1.80
feldspar	69.00	2.54	171.00	–0.60
calcite	48.10	2.71	12.00	0.20
CLAY(a)	85.00	2.56	59.00	24.00
CLAY(b)	86.00	2.54	76.00	29.00

The system in Eq. (29) is well posed, since $\mathbf{M}$ is a square matrix (i.e., the system of equations has five equations and five unknowns). In this case, assuming that the definition of the volumetric fractions followed an exact description of formation constituents as in Table 1, it is expected that use of the NNLS inversion method summarized in Eq. (25) provides a stable solution. The plots of the volumetric fractions in Figure 5a confirm the good performance of the inversion in yielding a stable solution. Comparison of facies description in Table 1 with individual plots of volume fractions reveals good depth correlation of lithotypes with

formation constituents. For instance, the display of the volumetric fraction of K-feldspar $\mathrm{V_{felds}}$ confirms the known arcosean nature of the sedimentary formation under study. A further example is the plot of the volumetric fraction of calcite $\mathrm{V_{calc}}$, confirming the carbonate-rich lithotype at the bottom of the formation.

The first and last displays in Figure 5a correspond to shaliness and effective porosity, respectively. In order to compare the results of distinct ways of estimating these properties, the display in Figure 6a shows the shaliness estimated by the mineral inversion and by the empirical model in Eq. (6), i.e., $\mathrm{V_{CLAY}}$ and $\mathrm{V_{CLAY}^{GR}}$, respectively. Interpretations are facilitated by additionally plotting the GR log. Due to the overestimation of shaliness by Larionov's empirical model in Eq. (6), significant differences are observed between both shaliness curves. These differences are even greater in the two major oil-producing sandstone intervals, because of the high radioactivity nature of the Namorado sandstone (Tigre & Lucchesi, 1986). Nevertheless, comparison of porosity curves in Figure 6b shows a very good match between the result of the mineral inversion and the use of Eq. (13), i.e., $\mathrm{V_{fluid}}$ and $\phi_{\mathrm{e,D}}$, respectively. The display of the ϕ_{N} log is also shown, as long as it helps interpretation and is required for shale point determination – see the procedure after Eq. (13). The discrepancies in Figure 6b between $\mathrm{V_{fluid}}$ and $\phi_{\mathrm{e,D}}$ are very small, pointing out the robustness of estimating effective porosity by means of the bulk density log. Note the insensitiveness of Eq. (13) to shaliness estimation from Larionov's empirical model in a high radioactivity sedimentary interval. The monomineralic assumption for the lithotypes (i.e., quartzoze rock matrix) seems to compensate for the shaliness overestimation using Larionov's empirical formula. Still concerning porosity estimation, use of Eq. (19) produced nearly the same result of Eq. (13) – not shown here. As a remark, note that in Eq. (19) $\mathrm{V_{CLAY}}$ corresponds to shaliness estimated by the mineral inversion displayed in Figure 5a.

Incorporating the volumetric fractions in Figure 5a and further required parameters in the petrophysical model in Eq. (1) provides the good fit between the calculated and measured bulk density log in Figure 6c. Deviations of calculations from measurements of bulk density log are very small, yielding negligible absolute errors and a high correlation coefficient $\mathrm{r} = 0.96$. The correlation of the plots in Figure 7 provides a better interpretation of the lithology at well NA04. In the two major oil-producing sandstone intervals, the plots in Figures 7c and 7d confirm the core log facies description of lithology constituents. In the following, the bulk density estimation process provides results relatively inferior due to the lack of well log information entering the inversion method.

Bulk density estimation

In this section, the experiment with the petrophysical model in Eq. (1) refers to a possibly practical application of estimating bulk density at the well surroundings. In other words, we assume our data set with no information on bulk density log measurements. As a result, after excluding the bulk density log from the data set, the vector in (27) takes the following form:

$$\mathbf{r} = \begin{bmatrix} \Delta\mathrm{t_{log,i}} & \mathrm{GR_{log,i}} & \phi_{\mathrm{N,log,i}} & 1 \end{bmatrix}^{\mathrm{T}}, \tag{30}$$

and the matrix $\mathbf{M}$ in Eq. (28) reduces to

$$\mathbf{M} = \begin{bmatrix} \Delta\mathrm{t_{fluid}} & \Delta\mathrm{t_{qtz}} & \Delta\mathrm{t_{felds}} & \Delta\mathrm{t_{calc}} & \Delta\mathrm{t_{CLAY}} \\ \mathrm{GR_{fluid}} & \mathrm{GR_{qtz}} & \mathrm{GR_{felds}} & \mathrm{GR_{calc}} & \mathrm{GR_{CLAY}} \\ \phi_{\mathrm{N,fluid}} & \phi_{\mathrm{N,qtz}} & \phi_{\mathrm{N,felds}} & \phi_{\mathrm{N,calc}} & \phi_{\mathrm{N,CLAY}} \\ 1 & 1 & 1 & 1 & 1 \end{bmatrix}. \tag{31}$$

As explained in the experiment of bulk density calibration above, the physical values corresponding to the elements of matrix $\mathbf{M}$ are gathered in Table 2. However, the elimination of bulk density log information from the data set prevented determining the shale point as described after Eq. (13). We then considered the physical properties for CLAY constituents, i.e., $\Delta\mathrm{t_{CLAY}}$, $\mathrm{GR_{CLAY}}$ and $\phi_{\mathrm{N,CLAY}}$, as the mean of the sonic log, the maximum of the gamma-ray log and the maximum of the neutron porosity log, respectively. This strategy provided the best values for mineral inversion stability – see CLAY(b) in Table 2. Hence, the linear system in Eq. (1) can thus be expressed as follows

$$\begin{bmatrix} \Delta\mathrm{t_{log,i}} \\ \mathrm{GR_{log,i}} \\ \phi_{\mathrm{N,log,i}} \\ 1 \end{bmatrix} = \begin{bmatrix} 185.00 & 55.500 & 69.000 & 48.100 & 86.00 \\ 0.00 & 1.000 & 171.000 & 12.000 & 76.00 \\ 1.00 & -0.018 & -0.006 & 0.002 & 0.29 \\ 1.00 & 1.000 & 1.000 & 1.000 & 1.00 \end{bmatrix} \times \begin{bmatrix} \mathrm{V_{fluid}} \\ \mathrm{V_{qtz}} \\ \mathrm{V_{felds}} \\ \mathrm{V_{calc}} \\ \mathrm{V_{CLAY}} \end{bmatrix}. \tag{32}$$

Unlike the experiment of bulk density calibration, the system in Eq. (32) is ill posed. Due to the elimination of bulk density log from the data set, there are less equations than unknowns to solve the system of linear equations for the volumetric fractions of the formation constituents. As expected, inversion of the linear system above using the NNLS method summarized in Eq. (25) provided less stable results. In comparison to the volumetric fractions in Figure 5a, the plots in Figure 5b show significant differences in $\mathrm{V_{CLAY}}$ and $\mathrm{V_{calc}}$ and slight discrepancies in $\mathrm{V_{felds}}$, $\mathrm{V_{qtz}}$ and $\mathrm{V_{fluid}}$. The significant differences in the plot of $\mathrm{V_{calc}}$ in Figure 5b suggests the importance of bulk density in estimating the volumetric fraction of calcite in the formation under study.

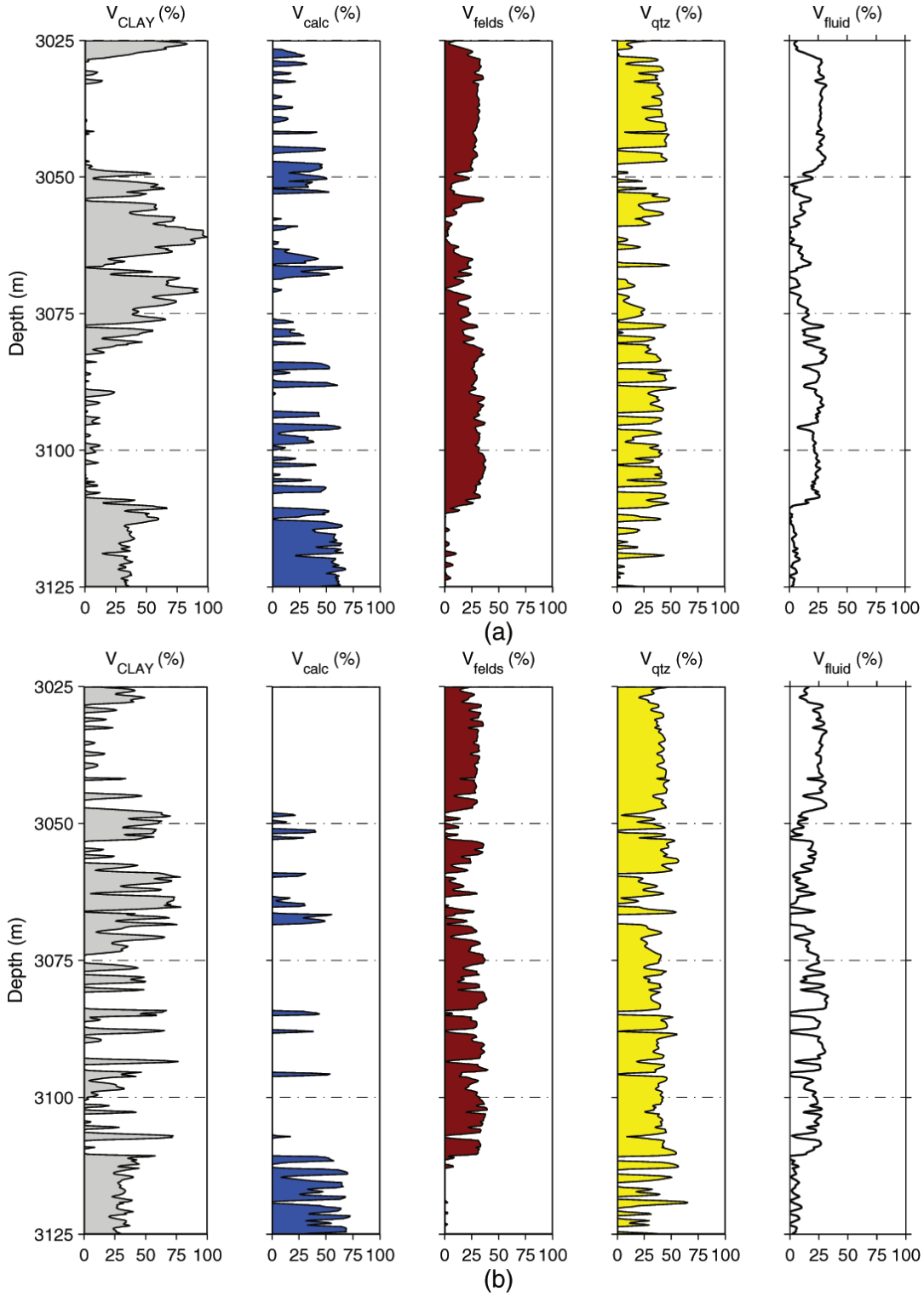

Figure 5 – Mineral volume inversion using the data set information of well NA04, which is formed by the well log measurements in Figure 3 and the facies description of core logs in Figure 4 (see Table 1). The terminology V_{CLAY}, V_{calc}, V_{felds}, V_{qtz} and V_{fluid} applies for the volumetric fractions of CLAY, calcite, feldspar, quartz and the flushed zone saturating fluid. In fact, V_{CLAY} and V_{fluid} correspond to shaliness and effective porosity, respectively. (a) Bulk density calibration experiment: the inversion of volumetric fractions included the Δt_ρ, ρ_b, GR and ϕ_N logs. (b) Bulk density estimation experiment: the inversion of volumetric fractions discarded the ρ_b log. Results are different because of the elimination of ρ_b log from the mineral volume inversion.

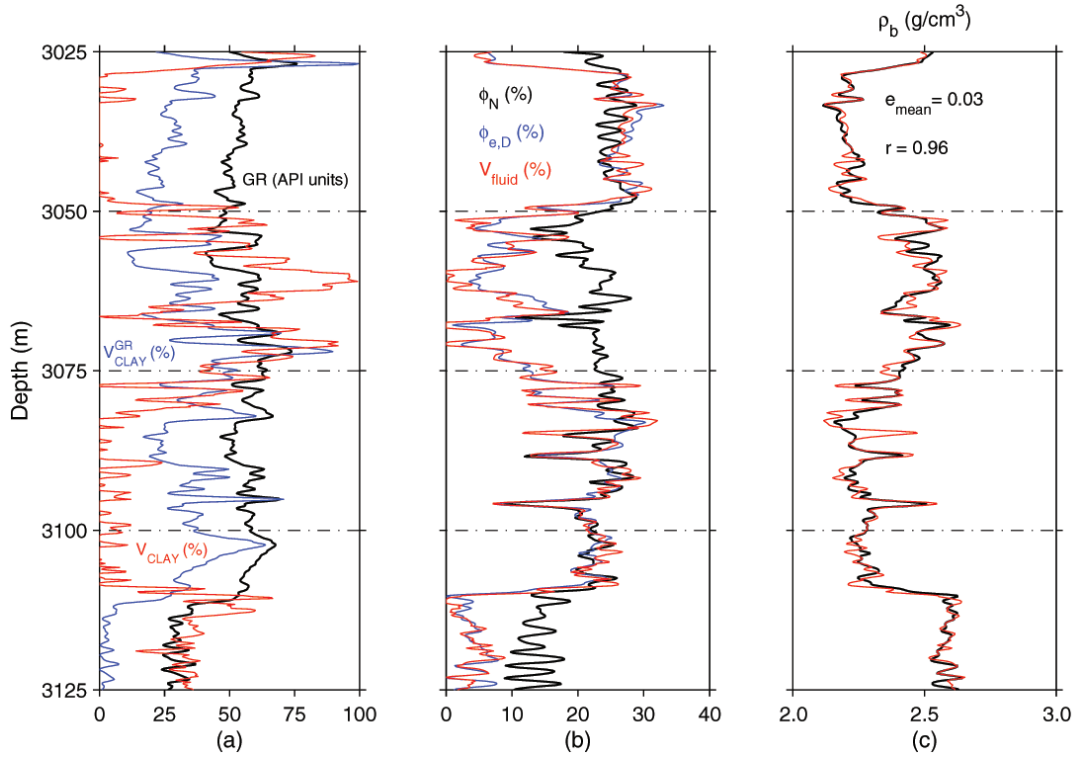

Figure 6 – Comparison of results obtained in the calibration process of bulk density log of well NA04. (a) Percentage of clay minerals $\mathrm{V_{CLAY}}$ (as in the first panel of Fig. 5a) estimated through mineral volume inversion, shaliness $\mathrm{V^{GR}_{CLAY}}$ according to Larionov's empirical formula in Eq. (6), and the GR log. (b) Fluid volume $\mathrm{V_{fluid}}$ (as in the last panel of Fig. 5a) estimated through mineral volume inversion, density-derived effective porosity $\phi_{\mathrm{e,\,D}}$ according to the formula in Eq. (13) and the ϕ_N log. Following the procedure after Eq. (13) for estimating $\phi_{\mathrm{e,\,D}}$, shaliness is taken as $\mathrm{V_{CLAY}} \equiv \mathrm{V^{GR}_{CLAY}}$; the bulk density at the shale point is $\rho_{\mathrm{CLAY}} = 2.56$ g/cm^3, $\rho_{\mathrm{ma}} \equiv \rho_{\mathrm{quartz}}$ and $\rho_{\mathrm{w}} \equiv \rho_{\mathrm{fluid}}$ are in Table 2. (c) Calibration of bulk density log at well NA04 using the petrophysical model in Eq. (1). Application of the petrophysical model took into account the volumetric fractions in Figure 5a and further required parameters in Table 2. The absolute errors between measurements (black curve) and the petrophysical model for bulk density (red curve) are negligible. Units are shown in the plots.

We point out that the differences between Figure 5a and Figure 5b could be minimized by replacing the bulk density log with any other available well log. However, our data set was limited to the well logs described in the beginning of this section.

As in Figure 6, the features in the plot of $\mathrm{V_{CLAY}}$ and $\mathrm{V_{fluid}}$ in Figure 5b are worth comparing. Although the features of $\mathrm{V_{CLAY}}$ in Figure 5a are different in Figure 5b, both plots show the remarkable presence of clay minerals in the upper Macaé formation. However, Figure 8a confirms once again the overestimation of shaliness using Larionov's empirical formula in Eq. (6). Radioactivity is very high in the main oil-producing sandstone intervals, leading to overestimation of shaliness through Larionov's empirical formula. In what concerns the comparison of the features in the porosity curves, we estimated the effective porosity using the $\Delta \mathrm{t}_P$ log. This procedure is justified by the assumption of no bulk density information in the data set. In Figure 8b, the plot of the sonic-derived porosity curve $\phi_{\mathrm{e,S}}$ almost matches $\mathrm{V_{fluid}}$. As pointed out in the literature (Dewan, 1983), use of sonic log overestimates porosity mainly in carbonate-rich lithologies. Moreover, the monomineralic assumption for $\phi_{\mathrm{e,S}}$ also seems to compensate for the overestimation of shaliness through Larionov's empirical formula in Eq. (6). Details on estimating $\phi_{\mathrm{e,S}}$ are in the caption of Figure 8b. As a further remark, the same comments apply if Eq. (19) is used for effective porosity estimation.

Using the volumetric fractions in Figure 5b and the additional required parameters in Table 2, the application of the petrophysical model in Eq. (1) yields the bulk density log in Figure 8c. The poor estimations provided by the mineral inversion method for $\mathrm{V_{CLAY}}$ and $\mathrm{V_{calc}}$ contributed to the major discrepancies observed between calculated and measured bulk density logs. However, considering the absolute mean error achieved and the relatively good correlation coefficient (i.e., $\mathrm{r} = 0.77$), the plot in Figure 8c shows preservation of the main features of the measured log. This result is also plotted in Figure 9, which confirms that the major discrepancies in bulk density log estimation correlates with poor estimations of $\mathrm{V_{CLAY}}$ and $\mathrm{V_{calc}}$ – see Figures 9c and 9d.

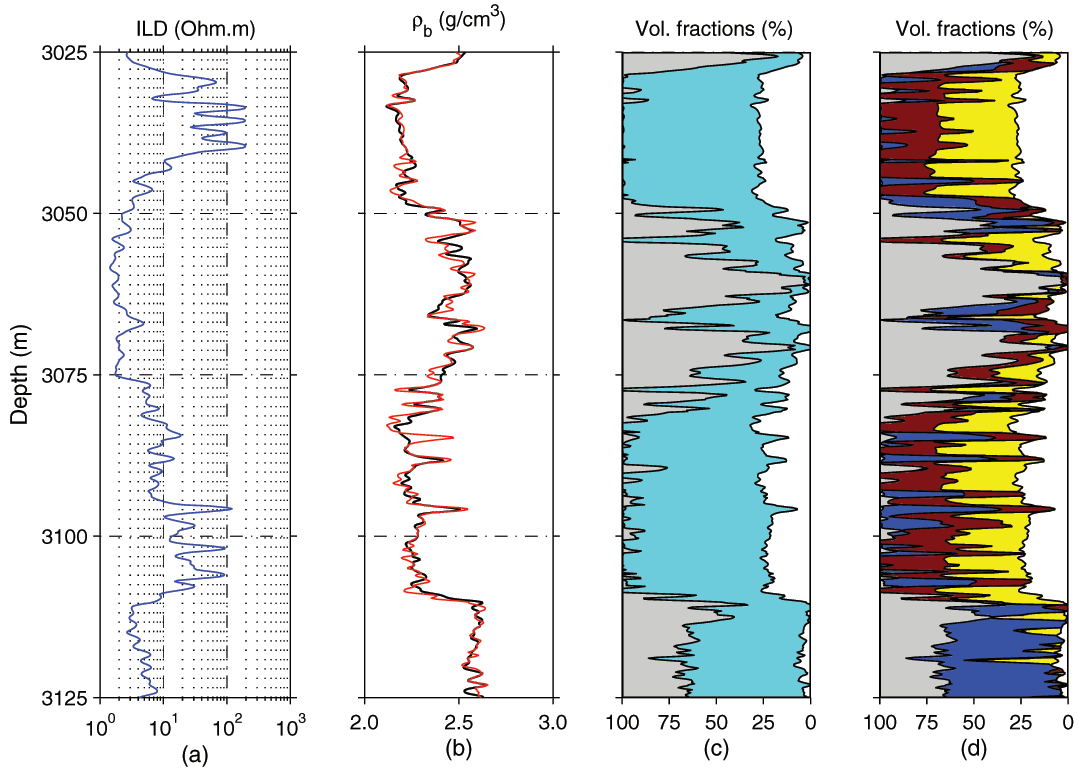

Figure 7 – Calibration of bulk density log at well NA04 using the petrophysical model in Eq. (1). (a) The R_{ild} log is displayed here for correlation of the two major oil-producing Namorado sandstone intervals with the main features of the plot of mineral volumetric fractions. (b) Comparison of measured log and petrophysical model for bulk density (red curve) as in Figure 6c. (c) Main rock constituents at well NA04: clay minerals (gray area), grain minerals (cian area) and effective porosity at well NA04. (d) Superposition of mineral volume fractions using the same color code as in Figure 5a. Note that only a qualitative interpretation of the induction electrical resistivity (R_{ild}) log in Figure 7a helps locating both highly radioactive, oil-producing sandstone intervals mentioned when describing the well log data set in Figure 3.

In the two oil-producing sandstone interval interpreted from the R_{ild} log (see Fig. 9a), the features of the measured bulk density log are preserved.

DISCUSSION AND CONCLUSIONS

The workflow of an integrated petrophysical analysis must incorporate tools for prediction of rock properties into the interpretation of well log measurements. Currently, most interpretation softwares rely on empirical models for rock property prediction. A set of core measurements from specific lithologies and a suitable mathematical formula are used in order to construct the empirical model by means of least-squares regression analysis. However, the application of the empirical model to other different lithologies may lead to significant misfits in the predictions. Only a mandatory uncertainty analysis can reveal if the selected mathematical formula is appropriate for describing the parameter dependence of the rock property under study. In other words, the conceptual model is crucial in the construction of petrophysical models with physically-consistent parameter dependence.

Based on the parallel layers concept, the conceptual model used in this paper for describing the bulk density of sedimentary rocks yielded a consistent petrophysical model. The main factors affecting bulk density measurements of rocks (i.e., the solid matrix, porosity and fluid content) are easily recognized as parameters of the dependence. For the application of the petrophysical model using well log measurements, the volumetric fractions of rock constituents and further physical parameters must be known beforehand. A data set containing facies description of lithotypes as well as a set of well log measurements helps defining the volumetric fractions of rock constituents for implementation of mineral volume analysis, while petrophysical tables give further physical parameters. In the presence of an insufficient number of well log measurements (i.e., underdetermined system of equations), the inversion algorithm for mineral volume analysis must necessarily incorporate constraints in order to avoid non-physical solutions.

The experiments in this paper showed the robustness of the petrophysical model in predicting bulk density well log measurements with negligible misfits and good correlation coefficient.

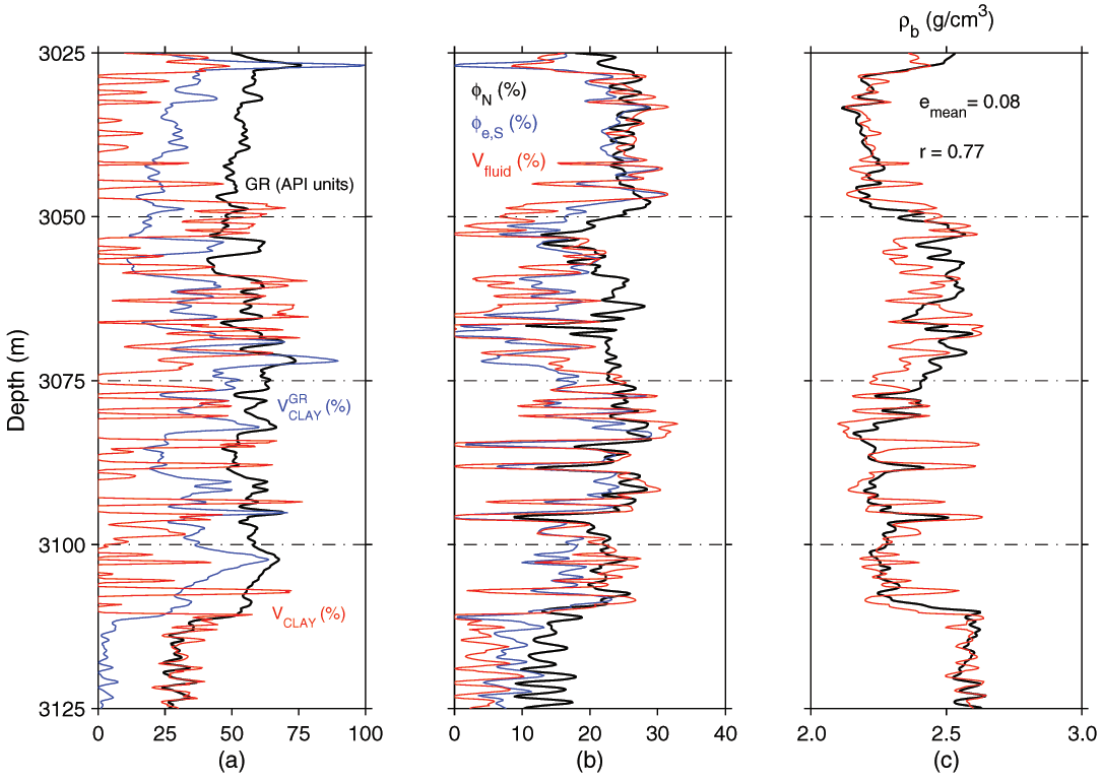

Figure 8 – Comparison of results obtained in the estimation process of bulk density log of well NA04. (a) Percentage of clay minerals V_{CLAY} (as in the first panel of Fig. 5b) estimated through mineral volume inversion, shaliness V^{GR}_{CLAY} according to Larionov's empirical formula in Eq. (6), and the GR log. (b) Fluid volume V_{fluid} (as in the last panel of Fig. 5b) estimated through mineral volume inversion, sonic-derived effective porosity $\phi_{e,S} = [(\Delta t_{qtz} - \Delta t\rho)/(\Delta t_{qtz} - \Delta t_{fluid})] - V^{GR}_{CLAY}[(\Delta t_{qtz} - \Delta t_{CLAY})/(\Delta t_{qtz} - \Delta t_{fluid})]$, and the ϕ_N log. Table 2 gives Δt_{CLAY}, Δt_{qtz} and Δt_{fluid}. (c) Estimation of bulk density log at well NA04 using the petrophysical model in Eq. (1). Application of the petrophysical model took into account the volumetric fractions in Figure 5b and further required parameters in Table 2. The absolute errors between measurements (black curve) and the petrophysical model for bulk density (red curve) are still negligible. Units are shown in the plots.

Such results suggest application of the parallel layers conceptual model to constructing petrophysical models for prediction of other well log measurements. In this instance, well log interpretations can benefit from incorporating these petrophysical models into an integrated analysis.

ACKNOWLEDGMENTS

Mariana Magalhães acknowledges support from FAPERJ – "Fundação Carlos Chagas Filho de Amparo à Pesquisa do Estado do Rio de Janeiro" (proc. no. E-26/100.172/2008), from PIBIC-ON/CNPq-MCT (proc. no. 101.583/2009-5) and from the Dept. of Geology, IGEO/UFF. This paper presents results of the research project "Caracterização de Anisotropia Sísmica Usando Perfis Geofísicos de Poços de Petróleo e Gás" with financial support from CNPq/Brazil, the Brazilian Agency for the Development of Sci. & Technology (proc. 471647/2006-3). Jorge L. Martins acknowledges a research scholarship from CNPq/Brazil (proc. 302480/2011-0). Preliminary results of this investigation were presented at the "III Simpósio Brasileiro de Geofísica", Belém, November 26-28, 2008.

REFERENCES

ARCHIE GE. 1942. The electrical resistivity log as an aid in determining some reservoir characteristics. Petroleum Trans., AIME, 146: 54–62.

ARCHIE GE. 1950. Introduction to petrophysics of reservoir rocks. Bulletin of the American Association of Petroleum Geologists, 34: 943–961.

AUGUSTO FOA & MARTINS JL. 2009. A well-log regression analysis for P-wave velocity prediction in the Namorado oil field, Campos Basin. Brazilian Journal of Geophysics, 27(4): 595–608.

BACKUS GE. 1962. Long-wave elastic anisotropy produced by horizontal layering. Journal of Geophysical Research, 67: 4427–4440.

CLAVIER C, COATES G & DUMANOIR J. 1977. The theoretical and experimental bases for the "dual water" model for the interpretation of shaly sands. Soc. of Professional Engineers of AIME: SPE 6859.

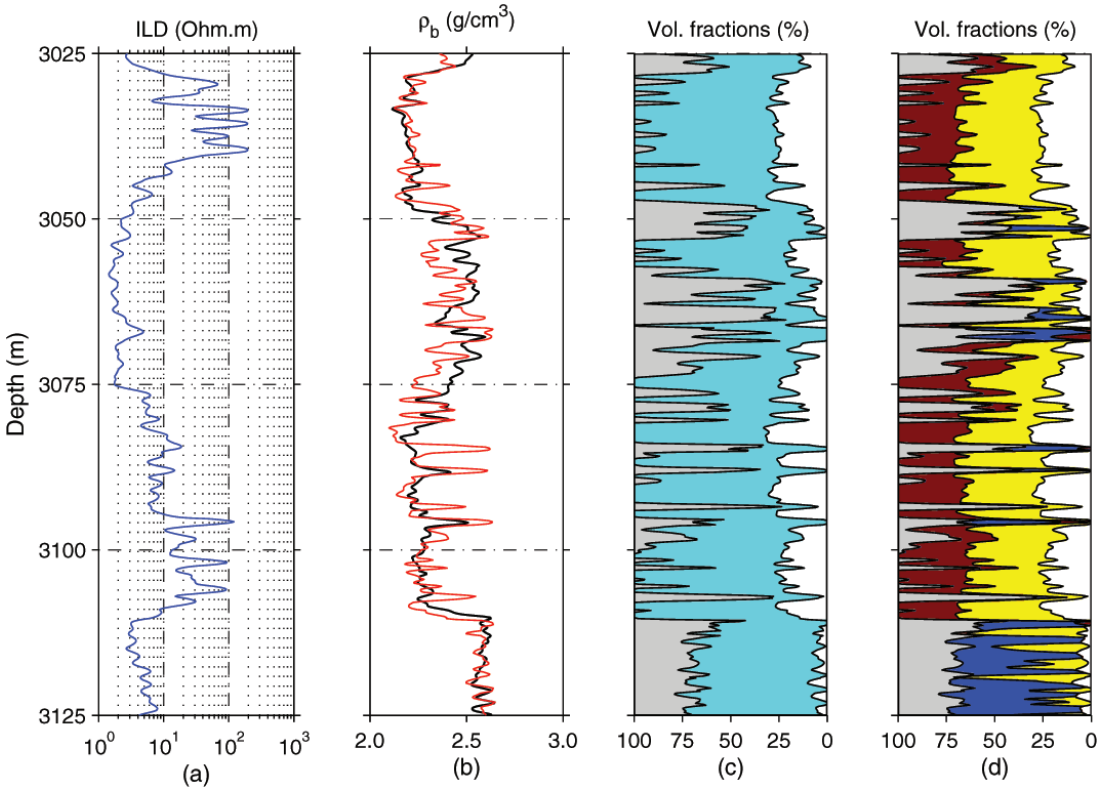

Figure 9 – Estimation of bulk density log at well NA04 using the petrophysical model in Eq. (1). (a) The same as in Figure 7a. (b) Comparison of measured log and petrophysical model for bulk density (red curve) as in Figure 8c. (c) Main rock constituents at well NA04: clay minerals (gray area), grain minerals (cian area) and effective porosity at well NA04. (d) Superposition of mineral volume fractions using the same color code as in Figure 5b. The inversion of mineral fractions ignored the measured bulk density log at well NA04 shown in Figure 3c.

DEWAN JT. 1983. Essentials of modern open-hole log interpretation. PennWell, 361 pp.

DOVETON JH. 1994. Geologic log analysis using computer methods. AAPG, Computer Applications in Geology, no. 2, 169 pp.

ELLIS DV & SINGER JM. 2007. Well logging for Earth scientists. 2nd edition. Springer, 692 pp.

LARIONOV WW. 1969. Borehole radiometry. Nedra, Moscow, 127 pp. (In Russian).

LAWSON CL & HANSON RJ. 1974. Solving least squares problems. Prentice-Hall, 340 pp.

LEVENBERG K. 1944. A method for the solution of certain nonlinear problems in least squares. Quarterly of Applied Mathematics, 2: 164–168.

LINER CL. 2004. Waves in porous solids. In: Elements of 3D seismology. 2nd edition. PennWell, Chapter 6: 135–152.

LINES LR & TREITEL S. 1984. A review of least-squares inversion and its application to geophysical problems. Geophysical Prospecting, 32: 159–186.

MAGALHÃES MF & MARTINS JL. 2008. Modelagem numérica da densidade efetiva de reservatórios de petróleo e gás. In: III Simpósio Brasileiro de Geofísica, 26-28 Novembro, Belém, CD-ROM. (In Portuguese).

MARQUARDT DW. 1963. An algorithm for least-squares estimation of nonlinear parameters. Journal of the Society for Industrial and Applied Mathematics, 11: 431–441.

PAIGE CC & SAUNDERS M. 1982. LSQR: An algorithm for sparse linear equations and sparse least squares. ACM Trans. Math. Software, 8: 43–71.

PENNINGTON WD. 2001. Reservoir geophysics. Geophysics, 66: 25–30.

POSTMA GW. 1955. Wave propagation in a stratified medium. Geophysics, 20: 780–806.

POUPON A & LEVEAUX J. 1971. Evaluation of water saturations in shaly formations. In: Trans. SPWLA 12th Annual Logging Symposium: Paper O1-2. (Full text in Shaly Sand Reprint Volume, SPWLA, Houston, pp IV, 81–95).

SCHÖN JH. 1996. Physical properties of rocks: Fundamentals and

principles of petrophysics. Handbook of Geophysical Exploration, Seismic Exploration. Pergamon, 18: 583 pp.

SIMANDOUX P. 1963. Measures dielectriques en milieu poreux, application a mesure des saturations en eau: Etude du comportement des massifs argileux. Revue de L'institut Français du Pétrole. Suplementary issue, 18: 193-215 (In French). (Full translated text in Shaly Sand Reprint Volume, SPWLA, Houston, pp. 97–124).

TIGRE CA & LUCCHESI CF. 1986. Estado atual do desenvolvimento da Bacia de Campos e perspectivas. In: Seminário de Geologia de Desenvolvimento e Reservatório, DEPEX-PETROBRAS, Rio de Janeiro, 1–12. (In Portuguese).

WYLLIE MRJ, GREGORY AR & GARDNER LW. 1956. Elastic wave velocities in heterogeneous and porous media. Geophysics, 21: 41–70.

WYLLIE MRJ, GREGORY AR & GARDNER LW. 1958. An experimental investigation of factors affecting elastic wave velocities in porous media. Geophysics, 23: 459–493.

NOTES ABOUT THE AUTHORS

Mariana Ferreira de Magalhães holds a B.S. degree (2009) in Geophysics and a post-graduation (specialization) degree (2011) in Petroleum Engineering from Universidade Federal Fluminense, Brazil. She has experience with seismic data processing. Currently, she works with Applied Geology and Geophysics. She is a member of SBGf.

Jorge Leonardo Martins holds a B.S. degree (1986) in Civil Engineering from Universidade Veiga de Almeida and a Ph.D. (1992) in Applied Geophysics from Universidade Federal da Bahia, Brazil. He was an associate researcher at Universidade Estadual do Norte Fluminense (1993-1998), visiting researcher at the Geophysical Institute of the Czech Academy of Science (April-June/1998), post-doctoral fellow at the SW3D Consortium Project (August/1998-January/2000), visiting researcher at Universidade Estadual de Campinas (2000), associate researcher at the Pontifícia Universidade Católica do Rio de Janeiro (2001), and visiting professor at Universidade do Estado do Rio de Janeiro (2002). Currently, he holds an associate researcher position at Observatório Nacional, Ministry of Science and Technology, Brazil. His professional interests include theory and practice of seismic anisotropy, azimuthal AVO analysis, integration of seismics with well log petrophysics, multicomponent seismics, and seismic data processing. He is a member of SEG and SBGf.